

## Effect of HCl and HNO<sub>3</sub> on the synthesis of pure and silver-based WO<sub>3</sub> for improved photocatalytic activity under sunlight

Priscila Hasse Palharim<sup>a,\*</sup>, Beatriz Lara Diego dos Reis Fusari<sup>a</sup>, Bruno Ramos<sup>a,b</sup>, Larissa Otubo<sup>c</sup>, Antonio Carlos Silva Costa Teixeira<sup>a</sup>

<sup>a</sup> Research Group in Advanced Oxidation Processes (AdOx), Department of Chemical Engineering, Escola Politécnica, University of São Paulo, Av. Prof. Luciano Gualberto tr. 3, 380, São Paulo, SP, Brazil

<sup>b</sup> Laboratory for Ceramics Processing, Department of Metallurgical and Materials Engineering, Escola Politécnica, University of São Paulo, Av. Prof. Mello Moraes, 2463, São Paulo, SP, Brazil

<sup>c</sup> Instituto de Pesquisas Energéticas e Nucleares (IPEN/CNEN), Cidade Universitária, Av. Prof. Lineu Prestes, 2242, São Paulo, SP, Brazil

### ARTICLE INFO

#### Keywords:

WO<sub>3</sub> photocatalysts  
Doped WO<sub>3</sub> photocatalysts  
Simulated sunlight  
Hydrothermal synthesis  
Photodegradation

### ABSTRACT

Heterogeneous photocatalysis have been considered an important and efficient alternative water and wastewater treatment process. In this area, different semiconductors, such as tungsten trioxide, have been investigated aiming to enhance photocatalytic performance. WO<sub>3</sub> is known to be an efficient material with high stability in acidic conditions. In the present work, pure and Ag/AgCl-doped WO<sub>3</sub> photocatalysts were synthesized by a simple hydrothermal method. A discussion of the effects of two pH-controlling agents, HCl and HNO<sub>3</sub>, in the final properties of the catalyst is reported for the first time. The materials were characterized by XRD, BET, SEM, EDS and UV–vis DRS. All catalysts showed similar or enhanced band gap values compared to a standard photocatalyst benchmark (TiO<sub>2</sub> P25). The type of acid did not lead to significant differences in morphology or photocatalytic activity of undoped catalysts. In contrast, doped catalysts prepared using HCl resulted in particles of flower-like morphology, with higher uniformity and slightly narrower band gap values. Furthermore, the use of HCl in the synthesis of silver-doped WO<sub>3</sub> resulted in catalysts containing AgCl, while Ag<sup>0</sup> was the major dopant species when HNO<sub>3</sub> was used. All materials exhibited good photocatalytic activity, with a maximum of 75.4% acetaminophen degradation under simulated sunlight achieved by the catalyst prepared with HCl and doped with 5% Ag-equivalent. For this catalyst, the degradation kinetics was found to be consistent with the Langmuir-Hinshelwood (L–H) model, and reusability tests showed no significant decrease in the degradation efficiency after four cycles. Finally, the effects of different scavengers suggest that O<sub>2</sub><sup>•−</sup> species play a major role in acetaminophen degradation with the material containing WO<sub>3</sub>, Ag and AgCl.

### 1. Introduction

Water contamination has become a great challenge due to the discharge of wastewater containing different classes of contaminants of emerging concern which, in some cases, cannot be completely removed by traditional wastewater treatment processes. Therefore, advanced oxidation processes, such as heterogeneous photocatalysis, have been considered important and efficient alternative treatment processes [1,2]. In this context, commercial TiO<sub>2</sub> has been the most widely applied catalyst for this purpose. Despite its low cost, the wide band gap energy (3.0–3.2 eV) and high charge recombination rate are viewed as important drawbacks. In fact, TiO<sub>2</sub> can only harvest UV radiation below 390

nm, which comprises only about 4–5% of the solar spectrum, therefore reducing its application with solar energy [2,3].

Consequently, different semiconductor photocatalysts have been investigated aiming to reduce the band gap energy and enhance light absorption, especially in the visible light region [4]. Tungsten trioxide (WO<sub>3</sub>) is a narrow band gap semiconductor with clear response to visible light (2.4–2.8 eV). It is considered an efficient material with high stability in acidic solutions [3,5]. Moreover, WO<sub>3</sub> is generally considered to exhibit photocatalytic activity for both the monoclinic and hexagonal crystalline phases [3]. Nevertheless, the photocatalytic activity of WO<sub>3</sub> is also seriously hindered by the recombination of photogenerated carriers, resulting in reduced process efficiency. This is explained by the

\* Corresponding author.

E-mail address: [ppalharim@usp.br](mailto:ppalharim@usp.br) (P. Hasse Palharim).

<https://doi.org/10.1016/j.jphotochem.2021.113550>

Received 28 November 2020; Received in revised form 20 August 2021; Accepted 13 September 2021

Available online 20 September 2021

1010-6030/© 2021 Elsevier B.V. All rights reserved.

WO<sub>3</sub> conduction band edge (about + 0.5 V vs. NHE) being more positive than the oxygen reduction potential ( $O_2/O_2^{\bullet-} = -0.33$  V vs. NHE), which inhibits the reduction reaction between photogenerated electrons in the conduction band (CB) of WO<sub>3</sub> and adsorbed oxygen molecules [6,7]. Therefore, it is important to modify the photocatalyst to allow the trapping of photogenerated electrons, so that holes in the valence band (VB) are available to oxidize the contaminant molecules rather than being consumed by recombination [6].

In order to overcome this problem, different methodologies have been applied such as morphological modifications [8–10], doping with metals and nonmetals [7,11–13], or combination of WO<sub>3</sub> with other materials to form heterojunctions [3,14–17]. Silver and silver-based materials are interesting options for doping and for producing heterojunctions with WO<sub>3</sub> catalysts, due to their low cost, high energy absorption in the visible spectrum and ability to enhance photocatalytic activity [3,5]. Some examples of silver-based materials that have been used as photocatalysts are Ag<sub>2</sub>S, Ag<sub>2</sub>WO<sub>4</sub>, Ag<sub>3</sub>PO<sub>4</sub>, Ag<sub>2</sub>MoO<sub>4</sub>, Ag<sub>2</sub>CO<sub>3</sub>, and AgX (X = Cl, Br and I) [18–24]. Among them, AgCl is an attractive material mainly because of its high visible light absorption capacity [25].

Conventionally, crystalline WO<sub>3</sub> can be synthesized through distinct approaches such as the hydrothermal method, sol-gel process, chemical vapor deposition, sputtering and anodization [11,26]. Each synthesis technique can produce materials with certain specific characteristics regarding elemental composition, crystalline structure and surface morphology. The main advantages of the hydrothermal process are the low cost compared with expensive vacuum technologies and the ease of handling [11]. In addition, this method allows for an easy control of morphology, size and crystallinity of the products [26].

The hydrothermal method has been applied to prepare WO<sub>3</sub> catalysts, with reported investigations on the influence of calcination temperature [4,7], presence of surfactants [27] and the influence of oxalic acid and pH in the synthesis [6,9]. Hydrochloric acid is the commonly used acidification agent in the synthesis of WO<sub>3</sub> catalysts with high stability [3,5]. Furthermore, different studies have used the hydrothermal method to synthesize doped WO<sub>3</sub> catalysts varying the dopant concentration and synthesis parameters [3,5,11,28,29]. Nevertheless, to the best of our knowledge, no systematic study has aimed at evaluating the effects of different acids in the synthesis step of photocatalysts using the one-step hydrothermal method. Also, few studies have estimated the degradation kinetics or the role of different oxidizing species on the degradation of organic contaminants using pure and silver-based WO<sub>3</sub> photocatalysts.

Hence, the current study aims to synthesize pure and doped WO<sub>3</sub> particles through a facile one-step hydrothermal method, evaluating the effect of type of acid (HCl or HNO<sub>3</sub>) used during the synthesis procedure at different pH values. The photocatalytic activities of the synthesized materials were evaluated in the heterogeneous photocatalytic degradation of acetaminophen (ACT), selected as a model contaminant. Finally, the degradation kinetics and the role of oxidizing species were investigated.

## 2. Materials and methods

### 2.1. Materials

Sodium tungstate dihydrate (Na<sub>2</sub>WO<sub>4</sub>·2H<sub>2</sub>O, ACS, ≥ 99%) and acetaminophen (HPLC, ≥ 99%) were purchased from Sigma-Aldrich. Concentrated hydrochloric acid (36–38% HCl), concentrated nitric acid (65% HNO<sub>3</sub>), silver nitrate (AgNO<sub>3</sub> ACS, PA) and ethanol were of analytical grade.

### 2.2. Synthesis of pure and doped WO<sub>3</sub>

Pure and doped WO<sub>3</sub> materials were synthesized via the one-step hydrothermal method. For synthesizing WO<sub>3</sub>, 15 mL of an aqueous

solution of 0.3-mol L<sup>-1</sup> Na<sub>2</sub>WO<sub>4</sub>·2H<sub>2</sub>O was prepared in Milli-Q® water (18.2 MΩ). Then, the pH was adjusted using HCl or HNO<sub>3</sub> to reach pH 0.5, 1.0 or 1.5, producing a total of six materials. Finally, this solution was transferred to a 220-mL PTFE-lined autoclave, which was kept in an oven at 120 °C for 24 h. The solid obtained was subsequently washed by resuspending and centrifuging for three times with ethanol and once with water to remove any possible ionic remnants. The final solution was dried in an oven at 80 °C for 24 h. Ag-doped WO<sub>3</sub> photocatalysts were synthesized by adding AgNO<sub>3</sub> to the 0.3 mol L<sup>-1</sup> Na<sub>2</sub>WO<sub>4</sub>·2H<sub>2</sub>O aqueous solution to achieve WO<sub>3</sub>-3% and 5% Ag (w/w). These solutions were kept under magnetic stirring for 1 h, at room temperature. Subsequently, the pH was adjusted to 1.5 using HCl or HNO<sub>3</sub>, resulting in four photocatalytic materials. Lastly, the materials were washed and dried as previously described. In addition, the WO<sub>3</sub>-5% Ag catalyst synthesized using HCl at pH 1.5 – thereafter named WO<sub>3</sub>-5% (HCl 1.5) – was calcined at 400 °C for 2 h to compare with the non-calcined catalyst.

### 2.3. Photocatalyst characterization

The morphology of the synthesized materials was investigated by scanning electron microscopy (SEM) and transmission electron microscopy (TEM). For the SEM analyses, a suspension of the sample in isopropanol was dripped on a silicon substrate and dried. Some observations were carried out in a SEM (Vega 3 LMU Tescan equipment), at 5 and 20 kV, and others in a FEG-SEM (JSM-6701F, Jeol) operating at 3 kV. For the TEM analyses, the suspension was dripped on a carbon coated copper grid and a JEM-2100 (Jeol) microscope was used, operating at 200 kV. The chemical composition was analyzed by energy dispersive X-ray spectroscopy (EDS) (Oxford equipment coupled to SEM). X-ray powder diffraction (XRD) patterns were obtained using a D8 Focus Bruker AXS equipment, at 20 kV and 40 mA with a Cu K-α radiation source and Ni filter. Ultraviolet–visible diffuse reflectance spectra (UV–vis DRS) were recorded on a spectrophotometer Shimadzu 2550, equipped with an integrating sphere. BET surface areas were measured by N<sub>2</sub> adsorption using a Gemini III 2375 equipment (Micromeritics Instrument Corp.).

### 2.4. Photocatalytic activity assays

Acetaminophen (ACT) was selected as a model contaminant to evaluate the photocatalytic activity of the synthesized materials. In a typical run, the catalyst (10 mg) was dispersed into 10 mL of 5-mg L<sup>-1</sup> ACT solution, in a 25-mL beaker. The reaction temperature was kept at 21 °C by using a thermal bath. First, the suspension was stirred in the dark for 90 min to achieve adsorption–desorption equilibrium. Then, photocatalytic experiments were conducted under simulated sunlight for 120 min, using a solar simulator (Peccell Inc., PEC-L01), with the light focus placed at 13 cm from the solution surface (Fig. S1). The irradiance was 3.4 mW cm<sup>-2</sup>, measured by a spectroradiometer (Luzchem, SPR-4002). 200-μL samples were collected over time, diluted five times, filtered and analyzed by HPLC. A HPLC Shimadzu LC20 chromatograph with a UV–vis detector (SPD20A), equipped with a C18 column (Prominent), was used to quantify ACT concentration. The mobile phase consisted of methanol:water (25:75), at a flow rate of 1.0 mL min<sup>-1</sup>; the injection volume and the temperature were 50 μL and 28 °C, respectively. The detection wavelength was 243 nm and the retention time was approximately 7 min. Under these conditions, the limits of ACT detection and quantification were 0.08 mg L<sup>-1</sup> and 0.24 mg L<sup>-1</sup>, respectively.

## 3. Results and discussion

### 3.1. Phase structure of the synthesized materials

Fig. 1a and 1b show the XRD patterns with indexed peaks of the pure

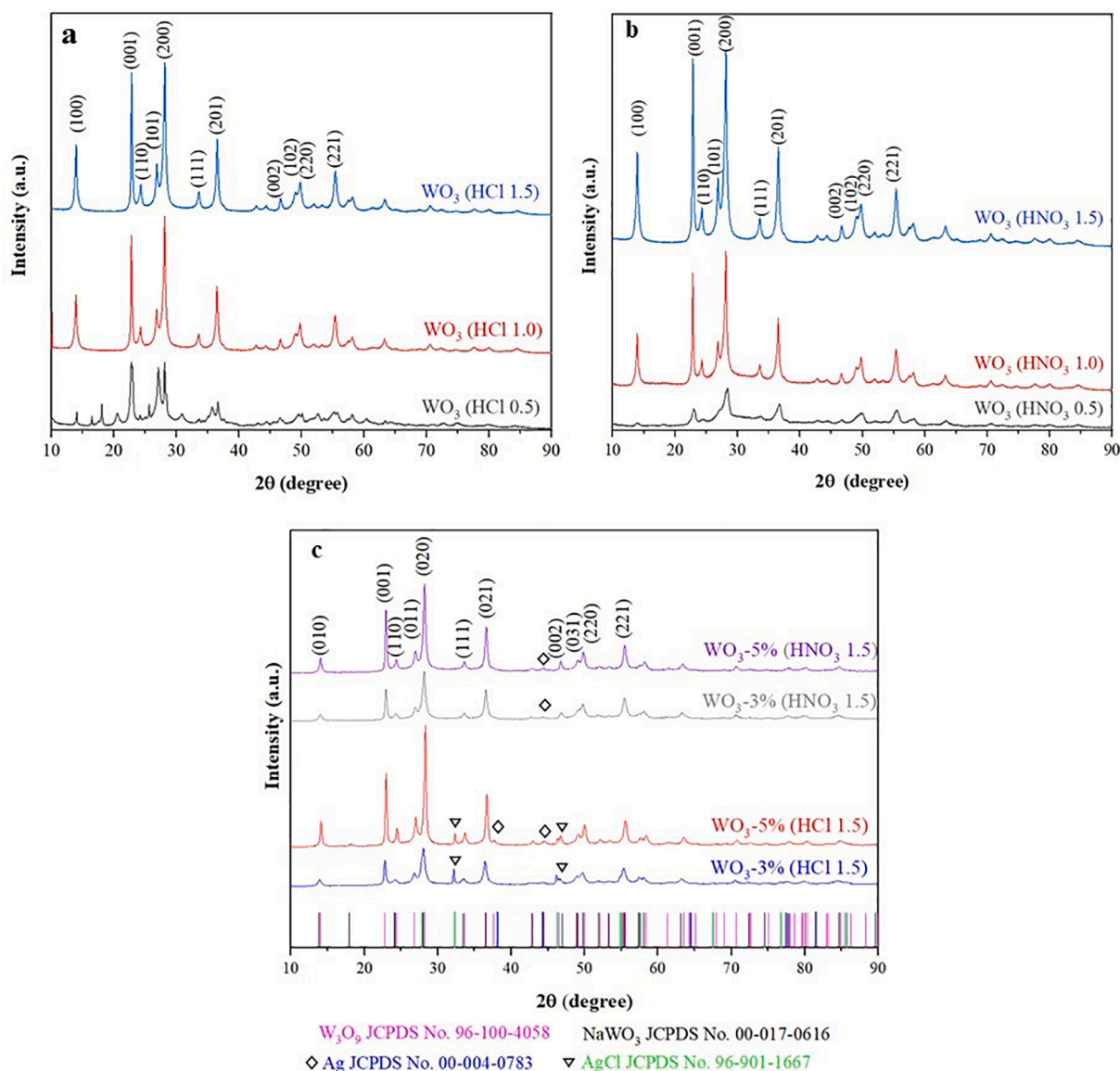


Fig. 1. XRD patterns of pure  $\text{WO}_3$  catalysts synthesized by the hydrothermal method using a) HCl at pH 0.5, 1.0, 1.5; b)  $\text{HNO}_3$  at pH 0.5, 1.0 and 1.5; and c) doped  $\text{WO}_3$  synthesized by the hydrothermal method using 3% and 5% of Ag with HCl or  $\text{HNO}_3$  at pH 1.5.

$\text{WO}_3$  catalysts synthesized at pH 0.5, 1.0 and 1.5, using HCl and  $\text{HNO}_3$ . Samples synthesized at pH 1.0 and 1.5 using HCl or  $\text{HNO}_3$  exhibited high crystallinity, with well-defined diffraction peaks. The XRD patterns were found to be a good match for the JCPDS Card No. 96-100-4058 of the  $\text{W}_3\text{O}_9$  hexagonal structure. Conversely,  $\text{WO}_3$  (HCl 0.5) particles seem to present more than one crystal structure. Likewise, in the case of  $\text{WO}_3$  ( $\text{HNO}_3$  0.5), the XRD pattern indicates the existence of diffraction peaks corresponding to the tungsten oxide anorthic phase (JCPDS Card No. 32-1395). Moreover, all XRD patterns showed to also match the JCPDS Card No. 00-017-0616 of sodium tungsten oxide hydrate.

Fig. 1c presents the XRD patterns of the doped  $\text{WO}_3$  particles, synthesized using HCl or  $\text{HNO}_3$  at pH 1.5. Again, the XRD patterns match the JCPDS Card No. 96-100-4058 of the  $\text{W}_3\text{O}_9$  hexagonal structure well. The addition of  $\text{AgNO}_3$  in the synthesis step resulted in different doped materials, depending on the acid used. For doped catalysts synthesized with  $\text{HNO}_3$ , although it is hard to identify extra peaks compared to the pure sample, the patterns were found to match the JCPDS Card No. 00-004-0783 of cubic metallic silver crystals [29]. However, HCl when used reacted with  $\text{AgNO}_3$  producing AgCl, whose diffraction peaks can be indexed to the cubic phase of AgCl (JCPDS Card No. 96-901-1667)

[3]. The most evident peaks appeared at  $2\theta$  of  $27.8^\circ$ ,  $32.24^\circ$ ,  $46.23^\circ$  and  $54.83^\circ$ , which are assigned to the crystallographic planes (1 1 1), (2 0 0), (2 2 0) and (3 1 1) of cubic AgCl. Hence, it is clear that the synthesized catalysts are composed of Ag, AgCl and  $\text{WO}_3$  particles. Also, it is evident that the intensity of diffraction peaks increases by increasing  $\text{AgNO}_3$  loading [11]. It is worth mentioning that  $\text{WO}_3$  is usually considered to show photocatalytic activity for hexagonal and monoclinic phases [3].

Crystallite sizes, calculated by the Scherrer equation (Table 1), did not show any clear trend with the type of acid used or dopant. The effect of crystallite size on photocatalytic performance is still questionable as the improvement in catalytic activity has been found to be related to the increase or decrease in crystallite size by different researchers [30]. Nandiyanto et al. [30] attribute the difficulty in understanding the correlation between crystallite size and activity to the different parameters that govern the photocatalytic process.

### 3.2. Morphological structure

Fig. 2 and Table 1 show the SEM images and the mean particle sizes, respectively, of the pure and doped  $\text{WO}_3$  catalysts. Fig. 2a-f reveal that

**Table 1**

N<sub>2</sub>-BET surface areas, crystallite size, SEM particle size, band gap energies and absorption edges of pure and doped WO<sub>3</sub> catalysts.

Catalyst	Crystallite size (nm)	Particle size (μm)	Surface area (m <sup>2</sup> g <sup>-1</sup> )	E <sub>g</sub> (eV)	λ <sub>g</sub> (nm)
WO <sub>3</sub> (HCl 0.5)	29.7	6.6 ± 3.6	51.69	2.98	416
WO <sub>3</sub> (HCl 1.0)	31.0	5.6 ± 3.7	66.37	2.86	433
WO <sub>3</sub> (HCl 1.5)	27.0	4.4 ± 2.6	34.28	2.64	469
WO <sub>3</sub> (HNO <sub>3</sub> 0.5)	9.9	5.5 ± 3.0	48.25	3.29	377
WO <sub>3</sub> (HNO <sub>3</sub> 1.0)	27.3	6.6 ± 2.2	60.12	3.32	373
WO <sub>3</sub> (HNO <sub>3</sub> 1.5)	24.9	5.6 ± 2.2	36.57	3.08	403
WO <sub>3</sub> -3% (HCl 1.5)	29.5	4.5 ± 1.8	23.68	2.91	426
WO <sub>3</sub> -3% (HNO <sub>3</sub> 1.5)	22.3	3.6 ± 1.8	37.59	2.79	444
WO <sub>3</sub> -5% (HCl 1.5)	19.8	4.0 ± 0.9	38.61	2.63	471
WO <sub>3</sub> -5% (HNO <sub>3</sub> 1.5)	27.2	4.6 ± 1.6	23.69	2.64	470
WO <sub>3</sub> -5% (HCl 1.5) - calcined	n.d.	n.d.	2.54	2.38	521

The % refers to the nominal silver content (w/w) of the catalyst.

bare WO<sub>3</sub> particles are irregularly shaped with mean particle sizes varying from 4.4 to 6.6 μm. In general, Ag-doping promoted a slightly decrease in particle sizes (Table 1). In contrast, the surface morphology of doped catalysts (Fig. 2g-k) is clearly more uniform compared to pure WO<sub>3</sub> catalysts, especially for those with 5% content of dopant. The variation in morphology reveals that the presence of Ag, especially as AgCl, influences WO<sub>3</sub> crystal growth [3].

Flower-like WO<sub>3</sub> particles can be observed in doped WO<sub>3</sub> samples, with mean particle sizes varying from 3.6 to 4.6 μm (Table 1). Despite having the same structural shape, the doped catalysts synthesized using HNO<sub>3</sub> (Fig. 2j-k) presented less uniform WO<sub>3</sub> morphology, suggesting that HNO<sub>3</sub> does not facilitate well-organized particle agglomeration. In turn, the doped WO<sub>3</sub> catalysts synthesized using HCl, particularly WO<sub>3</sub>-5% (HCl 1.5) (Fig. 2h-i) showed a highly uniform flower-like morphology; closer inspection shows that these flower-like structures are nanorod assemblies (Fig. 2i).

Similar structures are reported by Fang et al. [27], who synthesized WO<sub>3</sub> particles *via* the one-step hydrothermal method using HCl as acidification agent. The authors suggest that the better uniformity of the flower-like structures can be obtained with hydrothermal reaction times higher than 20 h, since the three-dimensional WO<sub>3</sub> nanostructures would grow gradually, resulting in flower-like structures. Therefore, the 24-h hydrothermal synthesis used in our study was clearly sufficient to promote the formation of flower-like structures. This structure formed by several nanorods can positively influence the photodegradation performance, when compared to compact spherical structures, for example. The slow photon effect may be a characteristic of this structure, which can improve the use of light [31].

A comparative assessment of the elemental mapping and the average chemical composition of the catalyst synthesized with 5% Ag was carried out by energy dispersive spectrometry (EDS). Both the elemental mapping and the EDS spectra, depicted in Fig. 3, confirm the presence of W and Ag on doped samples; similarly, Cl was found in the sample synthesized with HCl. No impurity peaks were observed. Interestingly, the WO<sub>3</sub>-5% (HNO<sub>3</sub> 1.5) catalyst has a highly uniform distribution of elements (Fig. 3b), suggesting that the WO<sub>3</sub> particles are consistently doped with silver. In contrast, the WO<sub>3</sub>-5% (HCl 1.5) catalyst presents Ag and Cl at specific sites (Fig. 3a), proving the formation of AgCl, as indicated by XRD analysis (Fig. 1c). In the scanned region, the WO<sub>3</sub>-5% (HCl 1.5) catalyst revealed 63.2% W, 14.1% Ag and 5.8% Cl; while the

WO<sub>3</sub>-5% (HNO<sub>3</sub> 1.5) catalyst showed 84.6% W and 15.4% Ag (atomic percentage).

The morphology of WO<sub>3</sub>-5% (HCl 1.5) catalyst was analyzed in detail by SEM-FEG. Fig. 4 shows the occurrence of smooth spherical-shaped particles with diameters ranging from 1 to 5 μm, which were confirmed as AgCl particles by EDS analyses. This suggests that the WO<sub>3</sub>-5% (HCl 1.5) catalyst is not completely uniform; instead, it is made of flower-like WO<sub>3</sub> and smooth spherical-shaped AgCl particles. Interestingly, it can be seen that AgCl particles are covered and/or in contact with WO<sub>3</sub> particles, forming a composite. Although this pattern is not commonly reported for the synthesis of WO<sub>3</sub>-AgCl, Chai et al. [32] successfully synthesized similar catalysts through the hydrothermal/photoreduction method, designating them as Ag-AgCl particles decorated with WO<sub>3</sub>.

In addition, WO<sub>3</sub>-5% (HCl 1.5) catalyst was also analyzed by TEM. Fig. 5a confirms that WO<sub>3</sub> particles are made of nanorods with length of 20 to 80 nm. It is possible to observe some small, spherical particles adhered to the WO<sub>3</sub> nanorods, which are confirmed to be metallic Ag, with particle diameters ranging from 9 to 37 nm. To better elucidate the presence of WO<sub>3</sub> and Ag, some selected areas were analyzed using high resolution TEM (Fig. 5b-c). The high crystallinity of the WO<sub>3</sub> nanorods is demonstrated by the clear lattice boundary in the HRTEM image (Fig. 5b). Two lattice spacings were found for the WO<sub>3</sub> phase, 3.65 Å and 6.25 Å, corresponding to the (001) and (010) crystalline planes of hexagonal W<sub>3</sub>O<sub>9</sub> (JCPDS Card No. 96-100-4058), corroborating the result obtained by XRD analysis. For the Ag phase (Fig. 5c), a lattice spacing of 2.36 Å was detected, which corresponds to the (111) crystalline plane of cubic metallic silver crystals (JCPDS Card No. 00-004-0783). Due to the large size of AgCl particles, their detection by HRTEM was not possible; even so, their presence was proved by SEM-FEG-EDS (Fig. 4). In conclusion, the SEM-FEG-EDS and TEM/HRTEM results indicate that the WO<sub>3</sub>-5% (HCl 1.5) photocatalyst is a composite consisting of Ag@WO<sub>3</sub>@AgCl, suggesting the formation of a complex heterojunction between these three materials.

### 3.3. BET surface areas

Table 1 presents the N<sub>2</sub>-BET specific surface areas of pure and doped WO<sub>3</sub> samples. Bare WO<sub>3</sub> catalysts have relatively large surface areas, with higher values shown for catalysts synthesized using HCl or HNO<sub>3</sub> at pH 1.0. The introduction of Ag into WO<sub>3</sub> promoted a slightly decrease in surface areas, which may be associated with increased particle agglomeration following silver incorporation. Pore blockage may also occur, causing a reduction in the surface area [33]. This result is consistent with the work of Yu et al. [3], which reported surface areas of 21 m<sup>2</sup> g<sup>-1</sup> and 5 m<sup>2</sup> g<sup>-1</sup> for samples of calcined WO<sub>3</sub> particles loaded with 0.25% and 1.25% AgCl, respectively.

For the catalysts synthesized using HNO<sub>3</sub>, increasing the Ag content resulted in lower surface areas, due to particle agglomeration. Conversely, for samples synthesized using HCl, an increase in the silver content led to an increase in the surface area. The complex Ag@WO<sub>3</sub>@AgCl structure may have contributed to the increase in surface area as more AgCl particles are available.

Note that the relatively high surface areas achieved are coherent with non-calcined WO<sub>3</sub> samples [10]. Hence, the WO<sub>3</sub>-5% (HCl 1.5) catalyst was calcined to compare with the non-calcined sample. From Table 1, it is clear that the calcination step drastically reduced the catalyst surface area. The higher calcination temperature promoted sintering of the particles, which could lead to pore collapse and/or blockage of smaller pores, thereby reducing the surface area and the pore volume as the pore diameter increased [34].

### 3.4. Optical properties

The UV-vis diffuse reflectance spectra of pure and doped WO<sub>3</sub> photocatalysts synthesized using HCl or HNO<sub>3</sub> at different pH values are

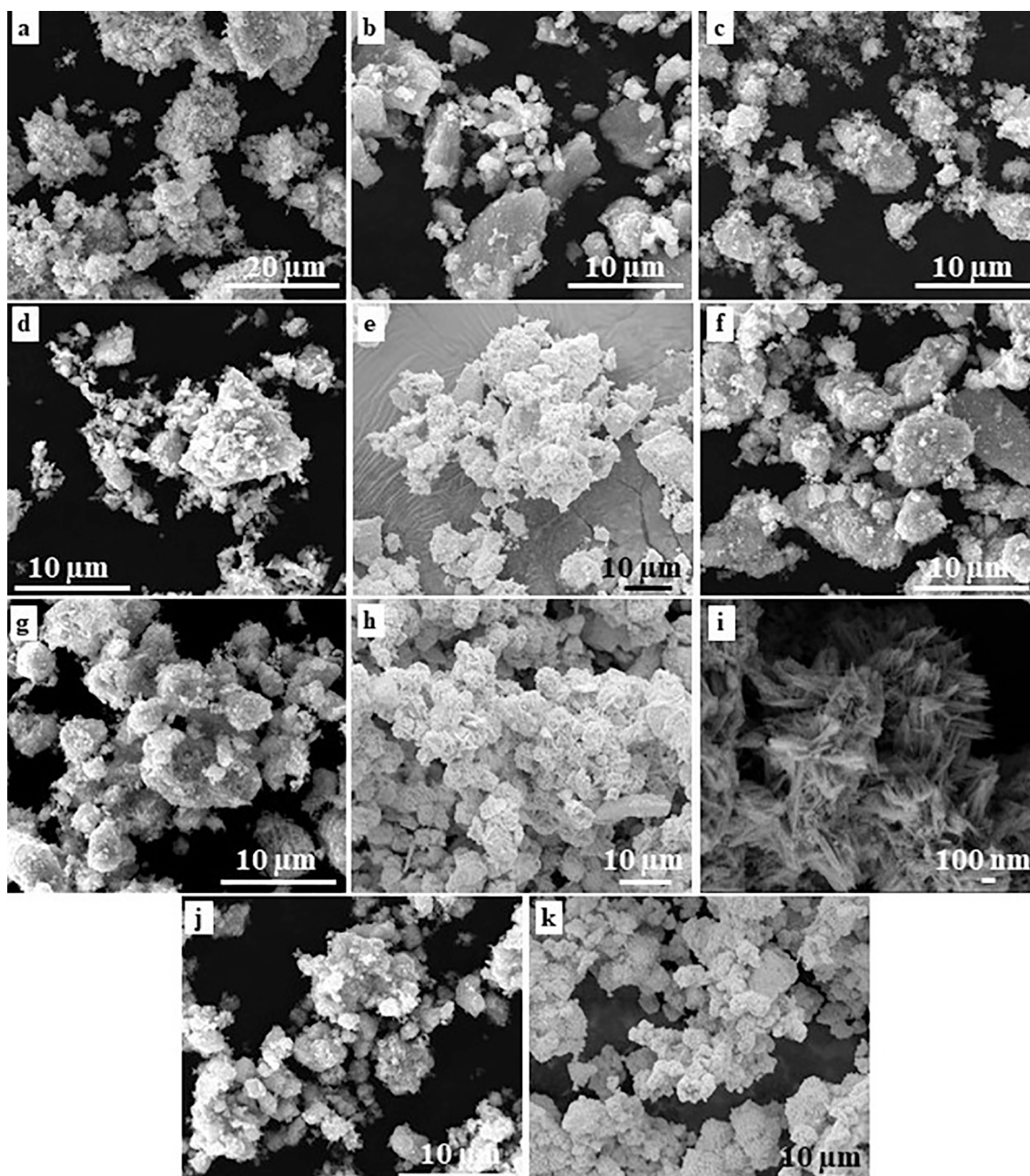


**Fig. 2.** SEM images of pure  $\text{WO}_3$  photocatalysts synthesized using  $\text{HCl}$  at pH a) 0.5, b) 1.0 and c) 1.5; pure  $\text{WO}_3$  photocatalysts synthesized using  $\text{HNO}_3$  at pH d) 0.5, e) 1.0 and f) 1.5; doped  $\text{WO}_3$  photocatalysts synthesized using  $\text{HCl}$  at pH 1.5 with g) 3% dopant and h-i) 5% dopant; doped  $\text{WO}_3$  photocatalysts synthesized using  $\text{HNO}_3$  at pH 1.5 with j) 3% dopant and k) 5% dopant.

displayed in Fig. 6. All the catalysts showed strong absorption in the UV region and considerable absorption of visible light, confirming their broad-spectrum activity. According to Yu et al. [10], the intrinsic band gap absorption of tungsten trioxide due to the electron transitions from the valence band to the conduction band ( $\text{O}_{2p} \rightarrow \text{W}_{5d}$ ) may have resulted in these absorption wavelengths. The coupling of Ag into  $\text{WO}_3$  slightly shifts the absorption edge to the visible light region.

The band gap energy was estimated by converting the diffuse reflectance spectra to the Kubelka-Munk function, and then extrapolating the linear slope of the curve to zero reflectance in the Tauc plot (Fig. S2). Table 1 shows that the  $E_g$  of all the samples was similar or enhanced when compared to commercial  $\text{TiO}_2$  (3.0–3.2 eV) [3,5], suggesting that the photocatalytic activity of the synthesized  $\text{WO}_3$  materials may be intensified under solar light. In general, there is no significant difference in the  $E_g$  values for the catalysts synthesized using  $\text{HCl}$  or

$\text{HNO}_3$ , yet those synthesized with  $\text{HNO}_3$  have slightly higher values. In contrast, the doped catalysts exhibited lower  $E_g$  values compared to the pure materials; also, the  $E_g$  values decreased with the increase of the silver content. The  $\text{WO}_3$ -5% ( $\text{HCl}$  1.5) catalyst was calcined to compare with the non-calcined sample. From Table 1, it can be seen that the calcination process resulted in a narrower band gap value and increased absorption in the visible range. Despite this being an advantage for photocatalysis, the surface area was found to be too low ( $2.54 \text{ m}^2 \text{ g}^{-1}$ ), which may reduce the photocatalyst activity.

The increase in the absorption edge observed for doped materials may be due to the localized surface plasmon resonance (LSPR) effect, as it allows the Ag nanoparticles to absorb light in the visible spectrum [35]. When LSPR occurs on the surface of the Ag nanoparticles excited by light, the radiated light is scattered and further absorbed on the Ag surface; as a result, an evanescent wave is generated with a strong

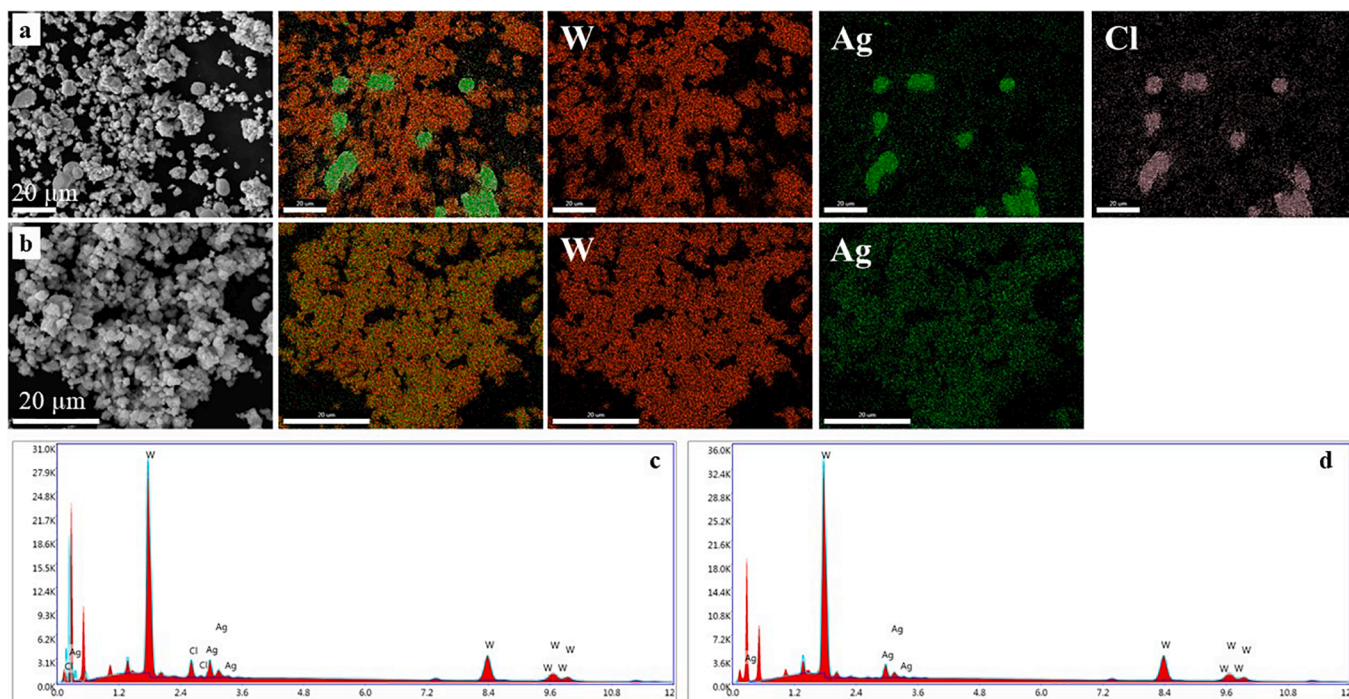


**Fig. 3.** Energy dispersive spectroscopy elemental mapping images and energy dispersive X-ray spectra (EDS) of a) and c)  $\text{WO}_3$ -5% (HCl 1.5) catalysts; b) and d)  $\text{WO}_3$ -5% ( $\text{HNO}_3$  1.5) catalysts.

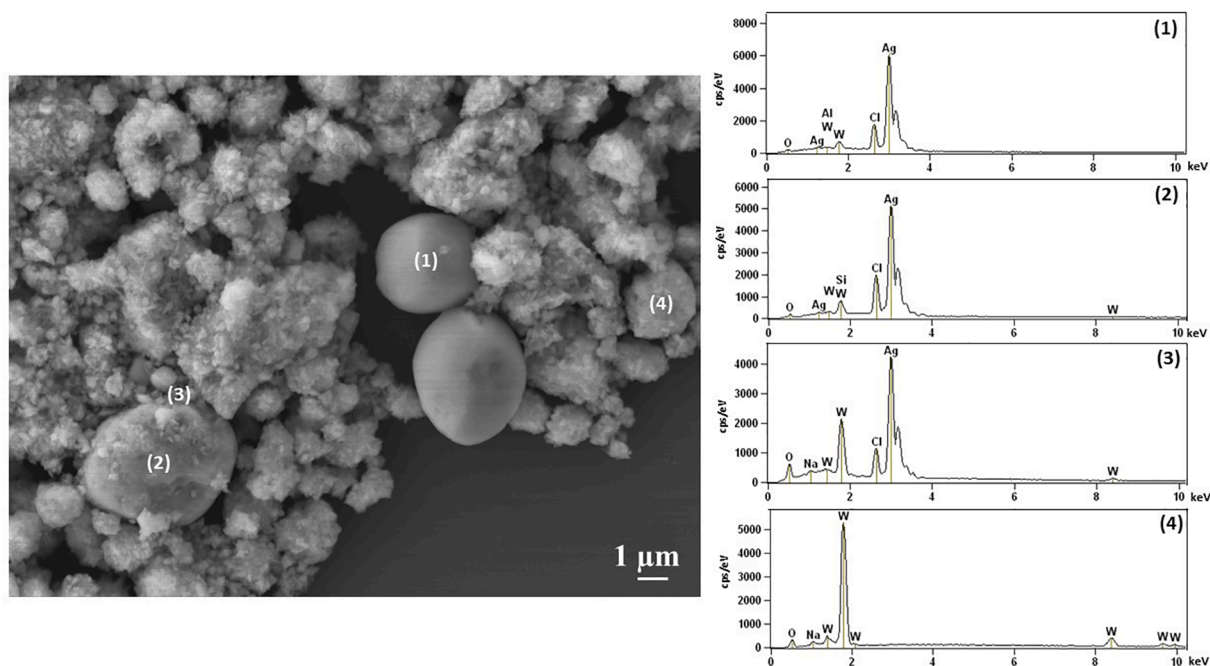


**Fig. 4.** SEM-FEG image of  $\text{WO}_3$ -5% (HCl 1.5) catalyst and corresponding energy dispersive X-ray spectra (EDS) at different sites.

electromagnetic field. This evanescent wave is localized on the Ag nanoparticle surface, rather than being propagated, and is kept at a distance from the surface less than the particle diameter. It is well known that LSPR contributes to the improvement of optical phenomena, such as light absorption and Raman scattering [36].

### 3.5. Photocatalytic activity

The photocatalytic performances of the pure and doped  $\text{WO}_3$

catalysts synthesized using HCl or  $\text{HNO}_3$  were evaluated by tracking the degradation of acetaminophen (ACT) under simulated sunlight. No appreciable ACT removal was observed during the first 90-min run under dark conditions. It can be seen from Fig. 7 that the pure  $\text{WO}_3$  photocatalysts showed poor activity upon ACT removal after 120 min of reaction, regardless of the acid (HCl or  $\text{HNO}_3$ ) used in their synthesis.

On the other hand, Ag-doped  $\text{WO}_3$  showed a largely improved ACT decomposition, particularly the samples synthesized with 5% content, which promoted the highest ACT degradation rates among all catalysts

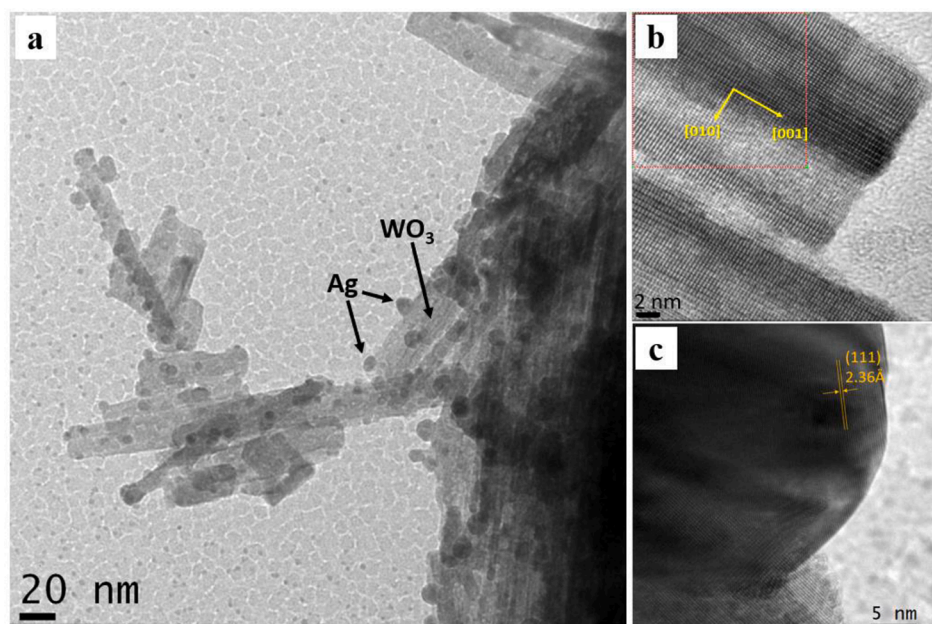


Fig. 5. (a) TEM and HRTEM images of  $\text{WO}_3$ -5% (HCl 1.5) catalyst showing crystal planes of (b)  $\text{WO}_3$  and (c) Ag.

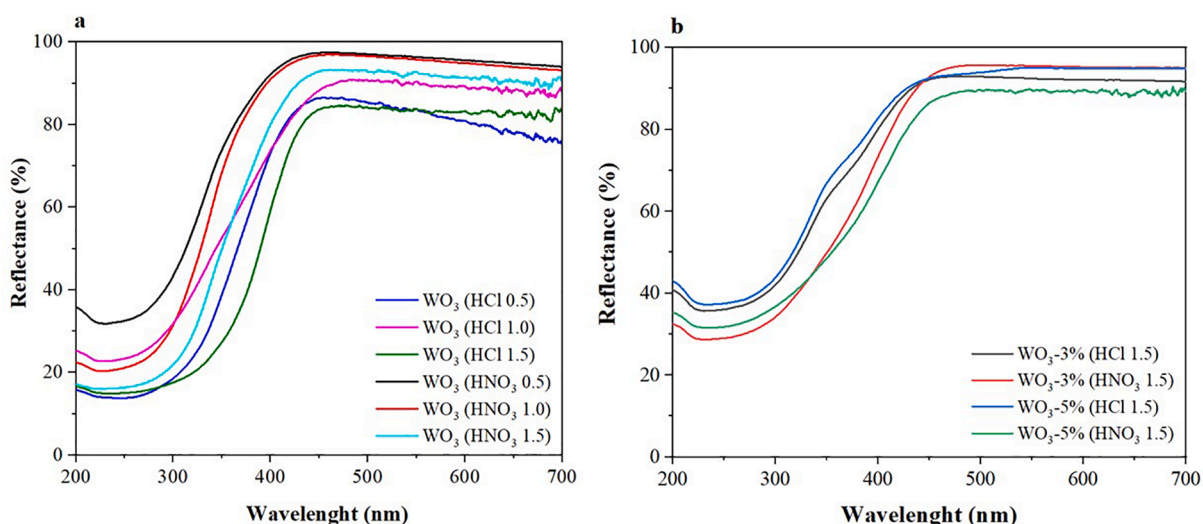


Fig. 6. UV-vis diffuse reflectance spectra of a) pure  $\text{WO}_3$  catalysts and b) doped  $\text{WO}_3$  catalysts synthesized using HCl or  $\text{HNO}_3$ .

tested. This behavior can be explained by the existence of a greater number of  $\text{Ag}^+$  ions available during the synthesis of the catalysts, leading to a combination of effects, among which the insertion of energy levels within the forbidden band, decreasing the band gap energy of particles with higher silver content [37], as seen in Table 1. Furthermore, as discussed previously, metallic Ag nanoparticles may form the SPR effect on the catalyst surface, increasing its ability to absorb visible light [36]. The doped catalysts synthesized with HCl exhibited better photocatalytic performance than the samples synthesized with  $\text{HNO}_3$ . This difference may be due to the presence of AgCl in the catalyst composite. As previously shown, the doped catalysts synthesized using HCl formed AgCl clusters, which can interact with  $\text{Ag@WO}_3$  particles, significantly enhancing photo-generated charge-carrier separation and, consequently, photocatalytic activity. It is important to emphasize that this result was not achieved with the catalysts synthesized with  $\text{HNO}_3$ , i. e., without the formation of AgCl particles. A more in-depth discussion of the degradation mechanism and role of AgCl will be discussed later in Section 3.8. The best result was achieved with the  $\text{WO}_3$ -5% (HCl 1.5)

catalyst, which degraded 75.4% of ACT after 120 min of reaction, following a kinetic behavior consistent with a pseudo first-order model, with a rate constant of  $0.0458 \text{ min}^{-1}$ . The degradation percentage achieved by all photocatalysts, along with the corresponding specific pseudo first-order degradation rates ( $k$ ), are summarized in Table 2. These results clearly show that the experimental data were well fitted to pseudo first-order kinetics, with the doped photocatalysts exhibiting considerable enhancement of the ACT degradation rates compared to the pure materials.

In order to evaluate the influence of the calcination process, the  $\text{WO}_3$ -5% (HCl 1.5) catalyst was calcined at  $200^\circ\text{C}$  for 2 h, and used in an additional degradation experiment for comparing with the non-calcined sample. The assay resulted in 77.3% degradation of ACT after 120 min of reaction, equivalent to a pseudo first-order kinetic constant of  $0.0422 \text{ min}^{-1}$ . No significant difference in the photocatalytic efficiency was thus observed between calcined and non-calcined samples, indicating that there is no need for thermal treatment following the synthesis procedure, therefore reducing its costs.

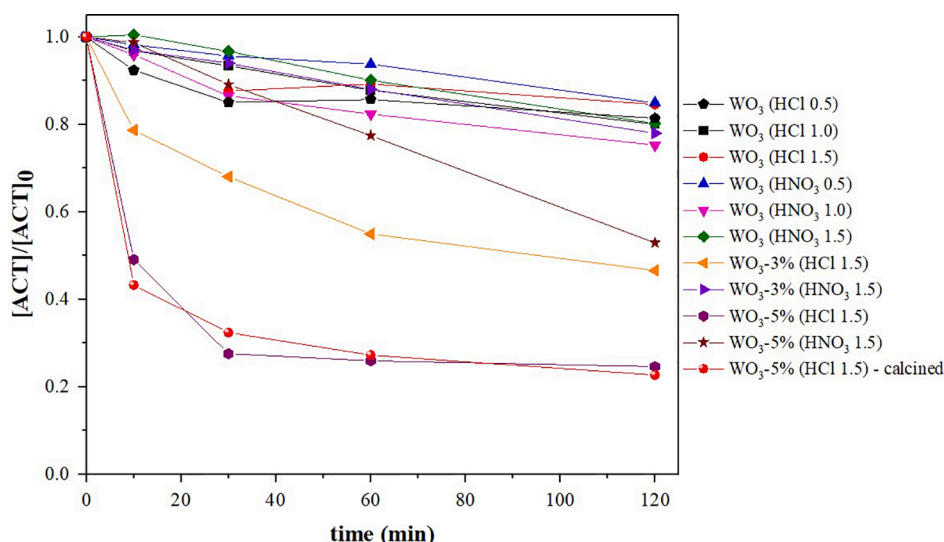


Fig. 7. Photocatalytic performance of pure and doped  $\text{WO}_3$  photocatalysts in the degradation of acetaminophen ( $[\text{ACT}]_0 = 5.03 \pm 0.09 \text{ mg L}^{-1}$ ) under simulated sunlight.

Table 2

ACT degradation rates and pseudo first-order kinetic constants for pure and doped  $\text{WO}_3$  catalysts.

Catalyst	ACT degradation (%) <sup>1</sup>	$k$ ( $\text{min}^{-1}$ ) <sup>2</sup>	$R^2$
$\text{WO}_3$ (HCl 0.5)	18.6	0.0057	0.983
$\text{WO}_3$ (HCl 1.0)	19.9	0.0024	0.986
$\text{WO}_3$ (HCl 1.5)	15.4	0.0015	0.982
$\text{WO}_3$ ( $\text{HNO}_3$ 0.5)	15.1	0.0013	0.992
$\text{WO}_3$ ( $\text{HNO}_3$ 1.0)	24.7	0.0048	0.998
$\text{WO}_3$ ( $\text{HNO}_3$ 1.5)	19.8	0.0018	0.993
$\text{WO}_3$ -3% (HCl 1.5)	53.3	0.0105	0.988
$\text{WO}_3$ -3% ( $\text{HNO}_3$ 1.5)	24.3	0.0024	0.991
$\text{WO}_3$ -5% (HCl 1.5)	75.4	0.0458	0.967
$\text{WO}_3$ -5% ( $\text{HNO}_3$ 1.5)	47.1	0.0050	0.991
$\text{WO}_3$ -5% (HCl 1.5) - calcined	77.3	0.0422	0.902

<sup>1</sup>After 120 min of reaction; <sup>2</sup>Calculated in the first 30 min of reaction.

The stability of the  $\text{WO}_3$ -5% (HCl 1.5) catalyst for ACT degradation was evaluated by reuse tests, which lasted 120 min, and were performed according to the photocatalytic experiments described in Section 2.4, starting with six runs. After each cycle, the photocatalysts were washed

by resuspension and centrifugation for three times with ethanol and once with water, then dried at  $80^\circ\text{C}$  for 24 h, and reused in the next run. For each run, the washed and dried photocatalysts were mixed to get a total of 10 mg. As seen in Fig. 8a, a small decrease in the photocatalytic activity was found, thus confirming the photocatalyst stability.

The XRD patterns of the fresh and used photocatalysts over four cycles are shown in Fig. 8b, and indicate that most of the peaks remain the same, except by an extra diffraction peak that appeared in the used catalyst. This peak, at  $2\theta = 38.1^\circ$ , is indexed to the (111) plane of cubic Ag (JCPDS Card No. 00-004-0783), indicating that  $\text{Ag}^+$  ions from AgCl were photo-reduced during the photocatalytic experiments [38]. It is known that an adequate  $\text{Ag}^0/\text{Ag}^+$  ratio is crucial for effective charge separation, playing an important role in the photocatalytic process. However, if this ratio is high, a silver cluster can be formed, becoming a charge-recombination center for the photogenerated carriers, hindering the photocatalytic activity [5]. Based on this, the small decrease in photocatalytic activity after four cycles can be explained by an increase in the  $\text{Ag}^0/\text{Ag}^+$  ratio or also by the moderately soluble nature of the  $\text{Ag}^+$  ions in the aqueous medium [5]. The XRD peaks confirm the chemical stability of the photocatalyst, a characteristic also noticed by Yu et al.

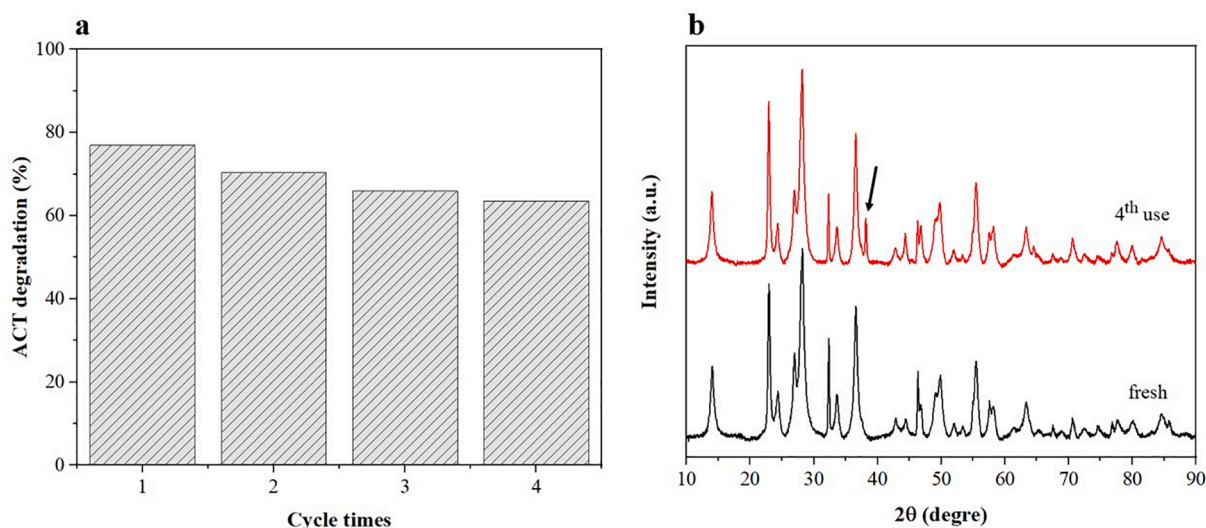


Fig. 8. (a) Reuse tests of the  $\text{WO}_3$ -5% (HCl 1.5), after 120 min; (b) XRD diffraction peaks of the fresh catalyst and after the 4<sup>th</sup> cycle of use.

[3], who reported that the comparatively high stability of doped  $\text{WO}_3$  photocatalysts is maintained, since the XRD patterns from fresh and reacted samples are similar after four runs.

### 3.6. Study of ACT degradation kinetics

For the evaluation of degradation kinetics, photocatalytic assays were performed with the  $\text{WO}_3$ -5% (HCl 1.5) material, which showed the best degradation performance, varying the initial ACT concentrations. Fig. 9a-b allow observing that the increase in the initial ACT concentration led to a decrease in the degradation efficiency. This result is expected, since an increase in the concentration of ACT molecules requires a proportional amount of  $\cdot\text{OH}$  and  $\text{O}_2^{\cdot-}$  radicals formed on the semiconductor surface in order to be oxidized. The generation rate and steady-state concentration of these species, however, remained the same, since fixed experimental conditions were used. As a result, the degradation efficiency decreased [39]. In addition, the photocatalyst might have been deactivated by the intermediate by-products formed from ACT degradation, which may be adsorbed onto the active sites and diffused from them at slower rates [39].

The Langmuir-Hinshelwood (L-H) expression was successfully (Fig. 9c) applied to model the photocatalytic degradation of ACT for the  $\text{WO}_3$ -5% (HCl 1.5) catalyst. The data were fitted to the linearized L-H model (Equation (1)), where  $k$  ( $\text{min}^{-1}$ ) is the pseudo first-order specific degradation rate,  $k_{\text{int}}$  ( $\text{mg L}^{-1} \text{min}^{-1}$ ) is the intrinsic reaction rate constant, and  $K_{\text{ACT}}$  ( $\text{L mg}^{-1}$ ) corresponds to the ACT adsorption constant onto the catalyst surface in the aqueous suspension. It is worth observing that the L-H equation can be approximated to the pseudo first-order kinetics when  $K_{\text{ACT}} \times C_0 \ll 1$  [40]. A satisfactory linear correlation was achieved ( $R^2 = 0.955$ ), with  $k_{\text{int}} = 0.288 \text{ mg L}^{-1} \text{ min}^{-1}$  and  $K_{\text{ACT}} = 0.113 \text{ L mg}^{-1}$ . It is important to mention that so far, degradation kinetic studies using  $\text{WO}_3$ -based photocatalysts have been limited to a few papers [41,42].

$$\frac{1}{k} = \frac{1}{k_{\text{int}}}[\text{ACT}]_0 + \frac{1}{k_{\text{int}}K_{\text{ACT}}} \quad (1)$$

### 3.7. Role of oxidizing species

During the photocatalytic degradation process, high reactive oxidizing species are generated from the interaction of adsorbed molecules with active holes and electron pairs generated on the irradiated semiconductor surface, which are essential for understanding the photocatalysis mechanism [43]. Among these species, it has been reported that superoxide radical anions ( $\text{O}_2^{\cdot-}$ ) and hydroxyl radicals ( $\cdot\text{OH}$ ), besides the holes ( $\text{h}^+$ ) themselves, are the main active [44]. Hence, additional experiments were performed to explore the effect of these species. For this, isopropanol, potassium iodide (KI), and 1,4-hydroquinone at

$0.02 \text{ mol L}^{-1}$  initial concentration each were selected as  $\cdot\text{OH}$ ,  $\text{h}^+$ , and  $\text{O}_2^{\cdot-}$  scavengers, respectively [43,45]. All the experiments lasted 60 min, and were performed using 10 mg of  $\text{WO}_3$ -5% (HCl 1.5) catalyst, 10 mL of ACT solution at  $5 \text{ mg L}^{-1}$  of initial concentration. So far, the effect of oxidizing species using  $\text{WO}_3$ -based photocatalysts has been explored by just a few works [46,47].

As shown in Fig. 10, when 1,4-hydroquinone was added to the reaction system, the photocatalytic degradation was completely suppressed, with the ultimate ACT percent removal plummeting from 64.8% in the absence of scavengers to 0%. This result suggests that  $\text{O}_2^{\cdot-}$  radical anions were the major reactive species in the photocatalytic degradation of ACT with the  $\text{WO}_3$ -based photocatalyst. When isopropanol was added to the system, the photocatalytic efficiency also suffered some suppression, with the ACT % removal after 60 min decreasing to 43.4%, which indicates that  $\cdot\text{OH}$  radicals play an important role as well, but are not the main radicals involved in the photo-degradation process.

Surprisingly though, when KI was added to the system, it accelerated ACT degradation, leading to an ultimate 92.7% ACT removal. A possible explanation for this result could be that the  $\text{h}^+$  scavenging effect of KI helped inhibiting charge recombination to some extent. Thus, surface-trapped electrons could participate in the degradation mechanism by contributing to the formation of other reactive species, or directly in the  $\text{O}_2$  reduction reaction (Equation (2)) [48] leading to the generation of  $\text{O}_2^{\cdot-}$  radicals, the major reactive species involved in ACT degradation. Finally, an extra experiment was conducted in which methanol was used to quench  $\text{h}^+$  [49]. In that case, Fig. 10 indicates that no significant difference in ACT degradation was observed in comparison with the experiment performed in the absence of scavengers, suggesting that  $\text{h}^+$  may not be relevant in the photocatalytic ACT degradation using the  $\text{WO}_3$ -5% (HCl 1.5) catalyst.



### 3.8. Photodegradation mechanism

A discussion of the degradation mechanism is presented for the  $\text{WO}_3$ -5% (HCl 1.5) catalyst, which resulted in the best ACT degradation. The valance and conduction bands of  $\text{WO}_3$  and AgCl were calculated through Equations (3) and (4), in which  $E_{\text{VB}}$ ,  $E_{\text{CB}}$ , and  $E_{\text{g}}$  refer to the potential of the valance and conduction bands, and the band gap energy, respectively;  $E^e$  denotes the energy of the free electron ( $\sim 4.5 \text{ eV}$ ), while  $\chi$  corresponds to the electronegativity of the materials, i.e., 6.59 and 6.08 eV for  $\text{WO}_3$  and AgCl, respectively [25].

$$E_{\text{VB}} = \chi - E^e + 0.5E_{\text{g}} \quad (3)$$

$$E_{\text{CB}} = E_{\text{VB}} - E_{\text{g}} \quad (4)$$

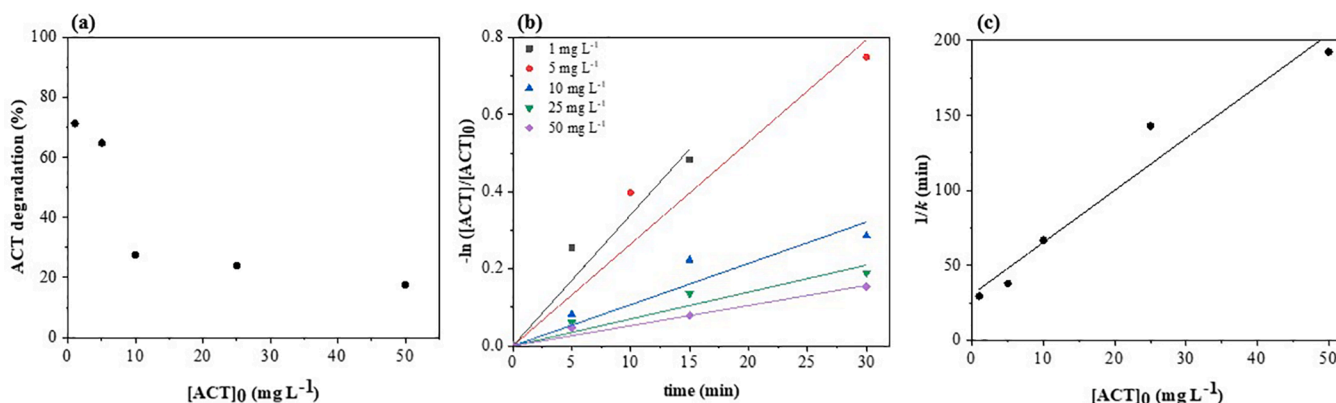
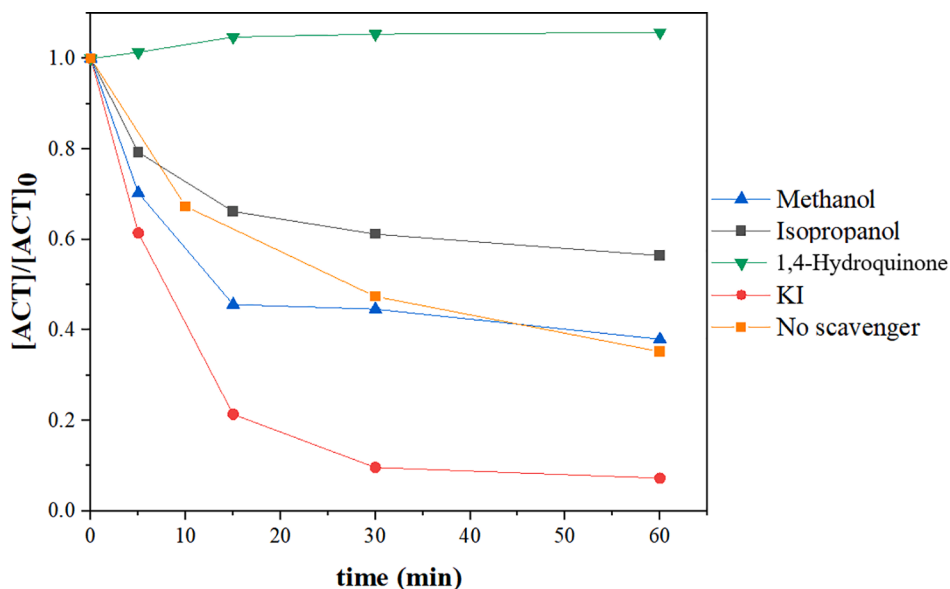


Fig. 9. (a) ACT degradation at various initial concentrations; (b) pseudo first-order kinetics; and (c) linearized L-H kinetics. All the experiments conducted using the  $\text{WO}_3$ -5% (HCl 1.5) catalyst.



**Fig. 10.** Effect of different radical scavengers on the efficiency of ACT degradation using  $\text{WO}_3$ -5% (HCl 1.5) catalyst. Conditions:  $[\text{ACT}]_0 = 5.02 \pm 0.12 \text{ mg L}^{-1}$ ;  $m_{\text{catalyst}} = 10 \text{ mg}$ ;  $V_{\text{solution}} = 10 \text{ mL}$ ; dosage of scavengers =  $0.02 \text{ mol L}^{-1}$ ; irradiation time = 60 min.

The VB and CB values for pure  $\text{WO}_3$  synthesized using HCl 1.5 were found to be 3.41 and 0.77 eV, respectively. The band values for AgCl were selected from literature, equal to 3.08 eV for VB and 0.07 eV for CB [25]. Thus, according to the band positions and the results mentioned so far, a possible mechanism for the degradation of ACT over the  $\text{WO}_3$ -5% (HCl 1.5) composite is proposed (Fig. 11). In accordance with the band gap energies, it is known that  $\text{WO}_3$  (2.64 eV - Table 1) can be excited by visible light, while AgCl (3.01 eV [3]) cannot; however, as a solar simulator was used in our photocatalytic experiments, AgCl may be excited by the UV portion of the spectrum [32]. Accordingly, AgCl and  $\text{WO}_3$  are excited to generate  $e^-/h^+$  pairs. As can be seen in the TEM images (Fig. 5), metallic silver was adhered to the surface of  $\text{WO}_3$ , and thus Ag particles may form the LSPR effect on the  $\text{WO}_3$  surface, enhancing its ability to absorb visible light [36]. In fact, the literature reports that  $\text{WO}_3$  is an effective LSPR host, which is associated with the

ability of its d valence-electrons to synergistically interact with silver [50]. Because the CB of AgCl is more negative than the CB of  $\text{WO}_3$ , and the VB of  $\text{WO}_3$  is more positive than that of AgCl, the photoexcited electrons in the AgCl conduction band can quickly transfer to the CB of  $\text{WO}_3$ . At the same time, the photo-generated holes in the VB of  $\text{WO}_3$  can migrate to the AgCl valence band. Consequently, the photo-generated  $e^-/h^+$  pairs can be successfully separated in the AgCl/ $\text{WO}_3$ -Ag composite.

The holes accumulated in the VB of AgCl can combine with  $\text{H}_2\text{O}$  ( $\text{H}_2\text{O}/\cdot\text{OH}$ : 2.72 eV vs. NHE) or  $\text{OH}^-$  ( $\text{OH}^-/\cdot\text{OH}$ : 2.40 eV vs. NHE) to form  $\cdot\text{OH}$  radicals, which play an important role in the photocatalytic ACT degradation [51]. Meanwhile, the electrons accumulated in the CB of  $\text{WO}_3$  cannot combine with  $\text{O}_2$  to form  $\text{O}_2^{\cdot-}$ , as this band potential is more positive than the standard potential of  $\text{O}_2^{\cdot-}$  ( $\text{O}_2/\text{O}_2^{\cdot-}$ : -0.33 eV vs. NHE) [32,51]. Likewise, even the electrons that may be in the CB of

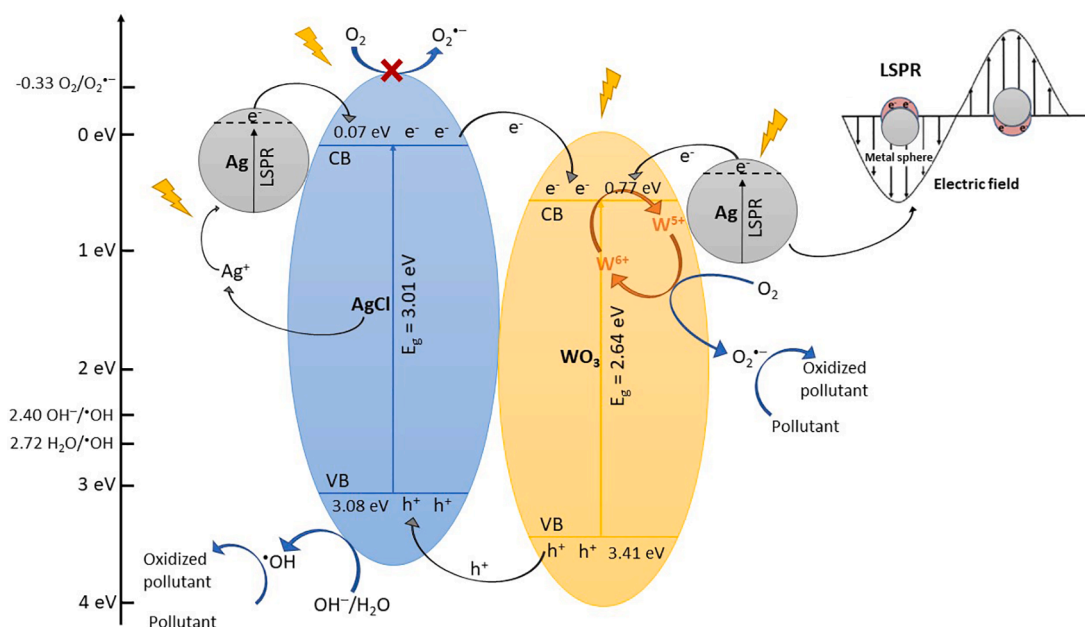


**Fig. 11.** Proposed photodegradation mechanism diagram of  $\text{WO}_3$ -5% (HCl 1.5) composite on the degradation of ACT under simulated sunlight irradiation.

AgCl cannot combine with O<sub>2</sub>. However, it was proven by the experiments with radical scavengers that O<sub>2</sub><sup>•-</sup> radicals are the most important reactive species in ACT degradation. Under these circumstances, we speculate the formation of W<sup>5+</sup> and W<sup>6+</sup> on the photocatalyst surface during the reaction. The hexagonal phase of WO<sub>3</sub> as found in this work can stimulate the transfer of electrons in the conduction band of semiconductor materials through the circulatory system between W<sup>5+</sup> and W<sup>6+</sup>, and as a consequence, convert these electrons into active species, increasing the activity of the photocatalyst [32]. Low-valence tungsten in the material can be excited by visible light, and high-valence tungsten is generated by loss of electrons [32]. Given that, Chai et al. [32] hypothesize that the W<sup>5+</sup> and W<sup>6+</sup> may be related to the generation of O<sub>2</sub><sup>•-</sup> radicals, considering that the electrons in the CB of WO<sub>3</sub> reduce W<sup>6+</sup> to W<sup>5+</sup>. Then, the electrons that were generated by the excitation of W<sup>5+</sup> have enough energy to reduce O<sub>2</sub> and thus produce O<sub>2</sub><sup>•-</sup>.

In addition, the XRD diffractogram of the used catalyst (Fig. 8b) confirms the formation of metallic Ag during the degradation process. Because of this, the generation of Ag<sup>0</sup> is proposed in Fig. 11, which can form the LSPR effect on the AgCl surface, contributing to its ability to absorb visible light. Finally, the composite made of AgCl and WO<sub>3</sub>-Ag may have formed an efficient heterojunction, where the active species O<sub>2</sub><sup>•-</sup> and •OH contribute to delaying charge-carrier recombination and increasing the photocatalytic activity of the synthesized material, comparing to bare WO<sub>3</sub>. This mechanism is useful to understand why the doped catalyst synthesized with HCl leads to greater photocatalytic activity than those prepared with HNO<sub>3</sub>. Particularly, AgCl particles and the interactions they can promote in the photocatalyst are fundamental for its performance, which may not be achieved with catalysts doped only with metallic Ag (i.e., synthesized with HNO<sub>3</sub>).

#### 4. Conclusions

In this work, pure and doped WO<sub>3</sub> photocatalysts were successfully synthesized by a facile one-step hydrothermal method, in which the particular effects of HCl or HNO<sub>3</sub> in the synthesis process were evaluated for the first time. For the pure WO<sub>3</sub> materials, HCl or HNO<sub>3</sub> did not lead to significant differences regarding morphology or photocatalytic activity.

However, doped catalysts produced using HCl resulted in particles of well uniform flower-like morphology, with higher uniformity compared to those produced using HNO<sub>3</sub>. Furthermore, when HCl was used, the catalysts resulted in a composite containing WO<sub>3</sub>, Ag and AgCl, while when HNO<sub>3</sub> was used, only Ag was the dopant. Yet, Ag played an important role in improving the degradation efficiency because of the LSPR effect.

The photocatalytic activity was markedly enhanced with the incorporation of AgCl and Ag to WO<sub>3</sub>, resulting in maximum acetaminophen degradation of 75.4% after 120 min with the WO<sub>3</sub>-5% (HCl 1.5) catalyst under simulated sunlight. Thus, the Langmuir-Hinshelwood (L-H) kinetic expression was successfully applied for this catalyst, resulting  $k_{int} = 0.288 \text{ mg L}^{-1} \text{ min}^{-1}$  and  $K_{ACT} = 0.113 \text{ L mg}^{-1}$ .

The stability evaluation showed that the synthesized materials were stable over four cycle runs, with no significant decrease in the degradation efficiency. Finally, the role of oxidizing species, evaluated by using different active species scavengers, revealed that O<sub>2</sub><sup>•-</sup> radical anions were the major reactive species in the photocatalytic degradation of ACT with the WO<sub>3</sub>-5% (HCl 1.5) photocatalyst. In this context, the formation of W<sup>5+</sup> and W<sup>6+</sup> on the photocatalyst surface was speculated to be related to the generation of O<sub>2</sub><sup>•-</sup> radicals.

#### CRedit authorship contribution statement

**Priscila Hasse Palharim:** Conceptualization, Methodology, Validation, Formal analysis, Investigation, Writing - original draft, Visualization. **Beatriz Lara Diego dos Reis Fusari:** Investigation. **Bruno Ramos:** Methodology, Formal analysis, Investigation, Writing - review & editing,

Supervision. **Larissa Otubo:** Formal analysis, Investigation. **Antonio Carlos Silva Costa Teixeira:** Validation, Resources, Writing - review & editing, Supervision, Funding acquisition.

#### Declaration of Competing Interest

The authors declare that they have no known competing financial interests or personal relationships that could have appeared to influence the work reported in this paper.

#### Acknowledgements

The authors express their gratitude to the São Paulo Research Foundation (FAPESP, grant no. 2018/21271-6), to the Brazilian National Council for Scientific and Technological Development (CNPq, grant no. 311230/2020-2) and to the Coordination for the Improvement of Higher Education Personnel – Brazil (CAPES) – Finance Code 001. The authors are also thankful to the Multiuser Central Facilities (UFABC), to the Electrochemistry and Corrosion Laboratory (ChE Department, USP), to the Laboratory for Technological Characterization - LCT (Mining and Petroleum Eng. Department, USP), to LapCat (ChE Department, USP) and to F. de J. Trindade for the support with materials characterization.

#### Appendix A. Supplementary data

Supplementary data to this article can be found online at <https://doi.org/10.1016/j.jphotochem.2021.113550>.

#### References

- [1] H. Zheng, J.Z. Ou, M.S. Strano, R.B. Kaner, A. Mitchell, K. Kalantar-zadeh, Nanostructured tungsten oxide - Properties, synthesis, and applications, *Adv. Funct. Mater.* 21 (12) (2011) 2175–2196, <https://doi.org/10.1002/adfm.v21.1210.1002/adfm.201002477>.
- [2] M.A. Suliman, M.A. Gondal, M.A. Dastageer, G.-K. Chuah, C. Basheer, Method for visible light-induced photocatalytic degradation of methylparaben in water using nanostructured Ag/AgBr@m-WO<sub>3</sub>, *Photochem. Photobiol.* 95 (6) (2019) 1485–1494, <https://doi.org/10.1111/php.v95.610.1111/php.13118>.
- [3] C. Yu, F. Chen, Z. Liu, K. Yang, H. Ji, D. Li, W. Xie, S. Li, Facile synthesis of a robust visible-light-driven AgCl/WO<sub>3</sub> composite microrod photocatalyst, *J. Alloys Compd.* 809 (2019) 151844–151854, <https://doi.org/10.1016/j.jallcom.2019.151844>.
- [4] H. Liu, C. Niu, H. Guo, C. Liang, D. Huang, L. Zhang, Y. Yang, L. Li, In situ constructing 2D/1D MgIn<sub>2</sub>S<sub>4</sub>/CdS heterojunction system with enhanced photocatalytic activity towards treatment of wastewater and H<sub>2</sub> production, *J. Colloid Interface Sci.* 576 (2020) 264–279, <https://doi.org/10.1016/j.jcis.2020.05.025>.
- [5] S. Adhikari, D. Sarkar, High efficient electrochromic WO<sub>3</sub> nanofibers, *Electrochim. Acta.* 138 (2014) 115–123, <https://doi.org/10.1016/j.electacta.2014.06.062>.
- [6] J.C. Murrillo-Sierra, A. Hernández-Ramírez, L. Hinojosa-Reyes, J.L. Guzmán-Mar, A review on the development of visible light-responsive WO<sub>3</sub>-based photocatalysts for environmental applications, *Chem. Eng. J. Adv.* 5 (2021) 100070–100091, <https://doi.org/10.1016/j.ceja.2020.100070>.
- [7] W. Mu, X. Xie, X. Li, R. Zhang, Q. Yu, K. Lv, H. Wei, Y. Jian, Characterizations of Nb-doped WO<sub>3</sub> nanomaterials and their enhanced photocatalytic performance, *RSC Adv.* 4 (2014) 36064–36070, <https://doi.org/10.1039/C4RA04080E>.
- [8] B. Ahmed, S. Kumar, A.K. Ojha, P. Donfack, A. Materny, Facile and controlled synthesis of aligned WO<sub>3</sub> nanorods and nanosheets as an efficient photocatalyst material, *Spectrochim. Acta Part A Mol. Biomol. Spectrosc.* 175 (2017) 250–261, <https://doi.org/10.1016/j.saa.2016.11.044>.
- [9] S.K. Biswas, J.-O. Baeg, S.-J. Moon, K.-J. Kong, W.-W. So, Morphologically different WO<sub>3</sub> nanocrystals in photoelectrochemical water oxidation, *J. Nanoparticle Res.* 14 (2012) 667–679, <https://doi.org/10.1007/s11051-011-0667-6>.
- [10] J. Yu, L. Qi, B. Cheng, X. Zhao, Effect of calcination temperatures on microstructures and photocatalytic activity of tungsten trioxide hollow microspheres, *J. Hazard. Mater.* 160 (2-3) (2008) 621–628, <https://doi.org/10.1016/j.jhazmat.2008.03.047>.
- [11] M.A.M. Khan, S. Kumar, T. Ahamad, A.N. Alhazaa, Enhancement of photocatalytic and electrochemical properties of hydrothermally synthesized WO<sub>3</sub> nanoparticles via Ag loading, *J. Alloys Compd.* 743 (2018) 485–493, <https://doi.org/10.1016/j.jallcom.2018.01.343>.
- [12] Y.-H. Xiao, C.-Q. Xu, W.-D. Zhang, Facile synthesis of Ni-doped WO<sub>3</sub> nanoplate arrays for effective photoelectrochemical water splitting, *J. Solid State Electrochem.* 21 (2017) 3355–3364, <https://doi.org/10.1007/s10008-017-3680-6>.
- [13] V. Rajendran, B. Deepa, Studies on the structural, morphological, optical, electrochemical and antimicrobial activity of bare, Cu and Ag @ WO<sub>3</sub> nanoplates by hydrothermal method, *J. Inorg. Organometallic Polym. Mater.* 28 (4) (2018) 1574–1586, <https://doi.org/10.1007/s10904-018-0846-3>.

- [14] H. Zhang, D. Yu, W. Wang, P. Gao, K. Bu, L. Zhang, S. Zhong, B. Liu, Multiple heterojunction system of  $\text{Bi}_2\text{MoO}_6/\text{WO}_3/\text{Ag}_3\text{PO}_4$  with enhanced visible-light photocatalytic performance towards dye degradation, *Adv. Powder Technol.* 30 (9) (2019) 1910–1919, <https://doi.org/10.1016/j.apt.2019.06.010>.
- [15] X. Zhao, X. Zhang, D. Han, L. Niu, Ag supported Z-scheme  $\text{WO}_2.9/\text{g-C}_3\text{N}_4$  composite photocatalyst for photocatalytic degradation under visible light, *Appl. Surf. Sci.* 501 (2020) 144258–144267, <https://doi.org/10.1016/j.apsusc.2019.144258>.
- [16] P. Jineesh, T.C. Bhagya, R. Remya, S.M.A. Shibli, Photocatalytic hydrogen generation by  $\text{WO}_3$  in synergism with hematite-anatase heterojunction, *Int. J. Hydrogen Energy.* 45 (38) (2020) 18946–18960, <https://doi.org/10.1016/j.ijhydene.2020.05.043>.
- [17] Y. Yang, X. Zhang, C. Niu, H. Feng, P. Qin, H. Guo, C. Liang, L. Zhang, H. Liu, L. Li, Dual-channel charges transfer strategy with synergistic effect of Z-scheme heterojunction and LSPR effect for enhanced quasi-full-spectrum photocatalytic bacterial inactivation: new insight into interfacial charge transfer and molecular oxygen activation, *Appl. Catal. B Environ.* 264 (2020) 118465–118480, <https://doi.org/10.1016/j.apcatb.2019.118465>.
- [18] X. Liu, J. Hu, J. Li, Y. Hu, Y. Shao, H. Yang, G. Tong, H. Qian, Facile synthesis of  $\text{Ag}_2\text{WO}_4/\text{AgCl}$  nanorods for excellent photocatalytic properties, *Mater. Lett.* 91 (2013) 129–132, <https://doi.org/10.1016/j.matlet.2012.09.078>.
- [19] J. Li, C. Yu, C. Zheng, A. Etogo, Y. Xie, Y. Zhong, Y. Hu, Facile formation of  $\text{Ag}_2\text{WO}_4/\text{AgX}$  (X = Cl, Br, I) hybrid nanorods with enhanced visible-light-driven photoelectrochemical properties, *Mater. Res. Bull.* 61 (2015) 315–320, <https://doi.org/10.1016/j.materresbull.2014.10.018>.
- [20] X. Zhao, L. Song, S. Zhang, Synthesis of  $\text{AgCl}/\text{Ag}_3\text{PO}_4$  composite photocatalysts and study on photodegradation activity based on a continuous reactor, *Photochem. Photobiol.* 94 (3) (2018) 484–490, <https://doi.org/10.1111/php.2018.94.issue-310.1111/php.12875>.
- [21] M. Geravand, F. Jamali-Sheini, Synthesis and physical properties of un- and Zn-doped  $\text{Ag}_2\text{S}$  nanoparticles, *Adv. Powder Technol.* 30 (2) (2019) 347–358, <https://doi.org/10.1016/j.apt.2018.11.012>.
- [22] S. Sousa, F. Xavier, E.A. Arau, J. Ricardo, R. Albuquerque, C. Couceiro, P. Røge, W. Ricardo, M. Elias, D. Matos, M. Rita, D.M. Chaves, Hydrothermal synthesis, structural characterization and photocatalytic properties of b- $\text{Ag}_2\text{MoO}_4$  microcrystals: Correlation between experimental and theoretical data, *Arab. J. Chem.* 13 (2020) 2806–2825, <https://doi.org/10.1016/j.arabjc.2018.07.011>.
- [23] M. Mahjoubian, A. Sadat, M. Sheykhan, Chemosphere Toxicological effects of  $\text{Ag}_2\text{O}$  and  $\text{Ag}_2\text{CO}_3$  doped  $\text{TiO}_2$  nanoparticles and pure  $\text{TiO}_2$  particles on zebra fish (*Danio rerio*), *Chemosphere.* 263 (2021) 128182–128196, <https://doi.org/10.1016/j.chemosphere.2020.128182>.
- [24] L. Li, C. Niu, H. Guo, J. Wang, M. Ruan, L. Zhang, C. Liang, H.-Y. Liu, Y.-Y. Yang, Efficient degradation of Levofloxacin with magnetically separable  $\text{ZnFe}_2\text{O}_4/\text{NCDs}/\text{Ag}_2\text{CO}_3$  Z-scheme heterojunction photocatalyst: Vis-NIR light response ability and mechanism insight, *Chem. Eng. J.* 383 (2020) 123192–123206, <https://doi.org/10.1016/j.cej.2019.123192>.
- [25] R.A. Senthil, S. Osman, J. Pan, M. Sun, A. Khan, V. Yang, Y. Sun, A facile single-pot synthesis of  $\text{WO}_3/\text{AgCl}$  composite with enhanced photocatalytic and photoelectrochemical performance under visible-light irradiation, *Colloids Surfaces A.* 567 (2019) 171–183, <https://doi.org/10.1016/j.colsurfa.2019.01.056>.
- [26] N. Li, T. Chang, H. Gao, X. Gao, L. Ge, Morphology-controlled  $\text{WO}_{3-x}$  homojunction: hydrothermal synthesis, adsorption properties, and visible-light-driven photocatalytic and chromic properties, *Nanotechnology.* 30 (2019) 415601–415612, <https://doi.org/10.1088/1361-6528/ab2a38>.
- [27] W. Fang, Y. Yang, H. Yu, X. Dong, T. Wang, W. Wang, Z. Liu, B. Zhao, M. Yang, One Step Synthesis of Flower-like  $\text{WO}_3$  Nanostructures for High Sensitivity Room Temperature NOx Gas Sensor, *RSC Adv.* 3 (2016) 106880–106886, <https://doi.org/10.1039/b000000x>.
- [28] M. Ahmadi, R. Younesse, M.-J.-F. Guinel, Synthesis of tungsten oxide nanoparticles using hydrothermal method at ambient pressure, *J. Mater. Res.* 29 (2014) 1424–1430, <https://doi.org/10.1557/jmr.2014.155>.
- [29] R. Ponnusamy, A. Gangan, B. Chakraborty, C.S. Rout, Tuning the pure monoclinic phase of  $\text{WO}_3$  and  $\text{WO}_3$ -Ag nanostructures for non-enzymatic glucose sensing application with theoretical insight from electronic structure simulations, *J. Appl. Phys.* 123 (2018) 024701–024710, <https://doi.org/10.1063/1.5010826>.
- [30] A.B.D. Nandiyanto, R. Zaen, R. Oktiani, Correlation between crystallite size and photocatalytic performance of micrometer-sized monoclinic  $\text{WO}_3$  particles, *Arab. J. Chem.* 13 (1) (2020) 1283–1296, <https://doi.org/10.1016/j.arabjc.2017.10.010>.
- [31] L. Su, L. Luo, J. Wang, T. Song, W. Tu, Z.-J. Wang, Lamellar flower-like porous  $\text{MoS}_2$  as an efficient cocatalyst to boost photocatalytic hydrogen evolution of CdS, *Catal. Sci. Technol.* 11 (4) (2021) 1292–1297, <https://doi.org/10.1039/D0CY02100H>.
- [32] C. Chai, J. Liu, Y. Wang, X. Zhang, D. Duan, C. Fan, Y. Wang, Enhancement in photocatalytic performance of Ag–AgCl decorated with h- $\text{WO}_3$  and mechanism insight, *Appl. Phys. A.* 125 (2019) 96–106, <https://doi.org/10.1007/s00339-019-2384-4>.
- [33] X. Zhu, H. Xu, Y. Yao, H. Liu, J. Wang, Y. Pu, W. Feng, S. Chen, Effects of  $\text{Ag}^0$ -modification and  $\text{Fe}^{3+}$ -doping on the structural, optical and photocatalytic properties of  $\text{TiO}_2$ , *RSC Adv.* 9 (68) (2019) 40003–40012, <https://doi.org/10.1039/C9RA08655B>.
- [34] Y. Ding, C. Zhao, Y. Li, Z. Ma, X. Lv, Effect of calcination temperature on the structure and catalytic performance of the Cu-MCM-41 catalysts for the synthesis of dimethyl carbonate, *Quim. Nova.* 41 (2018) 1156–1161, <https://doi.org/10.21577/0100-4042.20170291>.
- [35] K.H. Leong, B.L. Gan, S. Ibrahim, P. Saravanan, Synthesis of surface plasmon resonance (SPR) triggered Ag/ $\text{TiO}_2$  photocatalyst for degradation of endocrine disturbing compounds, *Appl. Surf. Sci.* 319 (2014) 128–135, <https://doi.org/10.1016/j.apsusc.2014.06.153>.
- [36] H. Jung, I. Yeo, T. Kim, H. Ki, H. Gu, Surface plasmon resonance effect of silver nanoparticles on a  $\text{TiO}_2$  electrode for dye-sensitized solar cells, *Appl. Surf. Sci.* 432 (2018) 266–271, <https://doi.org/10.1016/j.apsusc.2017.04.237>.
- [37] S. Ramkumar, G. Rajarajan, Enhanced visible light photocatalytic activity of pristine and silver (Ag) doped  $\text{WO}_3$  nanostructured thin films, *J. Mater. Sci. Mater. Electron.* 27 (11) (2016) 12185–12192, <https://doi.org/10.1007/s10854-016-5373-9>.
- [38] R.u. Qiao, M. Mao, E. Hu, Y. Zhong, J. Ning, Y. Hu, Facile formation of mesoporous  $\text{BiVO}_4/\text{Ag}/\text{AgCl}$  heterostructured microspheres with enhanced visible-light photoactivity, *Inorg. Chem.* 54 (18) (2015) 9033–9039, <https://doi.org/10.1021/acs.inorgchem.5b01303>.
- [39] M.J.N. Gotostos, C.C. Su, M.D.G. De Luna, M.C. Lu, Kinetic study of acetaminophen degradation by visible light photocatalysis, *J. Environ. Sci. Heal. - Part A Toxic/Hazardous Subst. Environ. Eng.* 49 (2014) 892–899, <https://doi.org/10.1080/10934529.2014.894310>.
- [40] K.V. Kumar, K. Porkodi, F. Rocha, Langmuir-Hinshelwood kinetics - A theoretical study, *Catal. Commun.* 9 (1) (2008) 82–84, <https://doi.org/10.1016/j.catcom.2007.05.019>.
- [41] C. Zhao, D. Li, Y. Liu, C. Feng, Z. Zhang, N. Sugiura, Y. Yang, Photocatalytic removal of microcystin-LR by advanced  $\text{WO}_3$ -based nanoparticles under simulated solar light, *Sci. World J.* 2015 (2015), <https://doi.org/10.1155/2015/720706>.
- [42] J. Rong, T. Zhang, F. Qiu, X. Rong, X. Zhu, X. Zhang, Preparation of hierarchical micro/nanostructured  $\text{Bi}_2\text{S}_3$ - $\text{WO}_3$  composites for enhanced photocatalytic performance, *J. Alloys Compd.* 685 (2016) 812–819, <https://doi.org/10.1016/j.jallcom.2016.06.210>.
- [43] D.B. Hernández-Uresti, D. Sanchez-Martinez, L.M. Torres-Martinez, Novel visible light-driven  $\text{PbMoO}_4/\text{g-C}_3\text{N}_4$  hybrid composite with enhanced photocatalytic performance, *J. Photochem. Photobiol. A Chem.* 345 (2017) 21–26, <https://doi.org/10.1016/j.jphotochem.2017.05.013>.
- [44] S. Deng, Z. Yang, G. Lv, Y. Zhu, H. Li, F. Wang, X. Zhang,  $\text{WO}_3$  nanosheets/ $\text{g-C}_3\text{N}_4$  rhodamine B, *Appl. Phys. A Mater. Sci. Process.* 125 (2019) 44–55, <https://doi.org/10.1007/s00339-018-2331-9>.
- [45] O. Fónagy, E. Szabó-Bárdos, O. Horváth, 1,4-Benzoquinone and 1,4-hydroquinone based determination of electron and superoxide radical formed in heterogeneous photocatalytic systems, *J. Photochem. Photobiol. A Chem.* 407 (2021) 113057–113071, <https://doi.org/10.1016/j.jphotochem.2020.113057>.
- [46] D. Zhang, J. Wang, In situ photoactivated plasmonic  $\text{Ag}_3\text{PO}_4$ @silver as a stable catalyst with enhanced photocatalytic activity under visible light, *Mater. Res.* 20 (2017) 702–711, <https://doi.org/10.1590/1980-5373-MR-2016-0800>.
- [47] D. Costenaro, C. Bisio, F. Carniato, A.M. Katsev, S.L. Safronyuk, N. Starodub, C. Tiozzo, M. Guidotti, Tungsten oxide: a catalyst worth studying for the abatement and decontamination of chemical warfare agents, *Glob. Secur. Heal. Sci. Policy.* 2 (2017) 62–75, <https://doi.org/10.1080/23779497.2017.1330662>.
- [48] J. Low, C. Jiang, B. Cheng, S. Wageh, A.A. Al-Ghamdi, J. Yu, A Review of Direct Z-Scheme Photocatalysts, *Small, Methods.* 1 (5) (2017) 1700080, <https://doi.org/10.1002/smt.d.v1.510.1002/smt.d.201700080>.
- [49] M. Shen, M.A. Henderson, Identification of the active species in photochemical hole scavenging reactions of methanol on  $\text{TiO}_2$ , *J. Phys. Chem. Lett.* 2 (21) (2011) 2707–2710, <https://doi.org/10.1021/jz201242k>.
- [50] Y. Yao, F. Ji, M. Yin, X. Ren, Q. Ma, J. Yan, S.F. Liu, Ag nanoparticle-sensitized  $\text{WO}_3$  hollow nanosphere for localized surface plasmon enhanced gas sensors, *ACS Appl. Mater. Interfaces.* 8 (28) (2016) 18165–18172, <https://doi.org/10.1021/acsami.6b04692>.
- [51] X. Yuan, L. Jiang, X. Chen, L. Leng, H. Wang, Z. Wu, T. Xiong, J. Liang, G. Zeng, Highly efficient visible-light-induced photoactivity of Z-scheme  $\text{Ag}_2\text{CO}_3/\text{Ag}/\text{WO}_3$  photocatalysts for organic pollutant degradation, *Environ. Sci. Nano.* 4 (11) (2017) 2175–2185, <https://doi.org/10.1039/C7EN00713B>.